

# Contrast-dependent saturation adjustment for outdoor image enhancement

SHUHANG WANG,<sup>1</sup> WOON CHO,<sup>2</sup> JINBEUM JANG,<sup>3</sup> MONGI A. ABIDI,<sup>2</sup> AND JOONKI PAIK<sup>3,\*</sup>

<sup>1</sup>Schepens Eye Research Institute, Mass Eye and Ear, Harvard Medical School, Boston, Massachusetts 02114, USA

<sup>2</sup>The Imaging, Robotics, and Intelligent Systems Laboratory, Department of Electrical Engineering and Computer Science, University of Tennessee, Knoxville, Tennessee 37996, USA

<sup>3</sup>Image Processing and Intelligent System Laboratory, Graduate School of Advanced Imaging Science and Film, Chung-Ang University, Seoul 06974, South Korea

\*Corresponding author: paikj@cau.ac.kr

Received 19 August 2016; revised 11 November 2016; accepted 14 November 2016; posted 14 November 2016 (Doc. ID 273985); published 5 December 2016

Outdoor images captured in bad-weather conditions usually have poor intensity contrast and color saturation since the light arriving at the camera is severely scattered or attenuated. The task of improving image quality in poor conditions remains a challenge. Existing methods of image quality improvement are usually effective for a small group of images but often fail to produce satisfactory results for a broader variety of images. In this paper, we propose an image enhancement method, which makes it applicable to enhance outdoor images by using content-adaptive contrast improvement as well as contrast-dependent saturation adjustment. The main contribution of this work is twofold: (1) we propose the content-adaptive histogram equalization based on the human visual system to improve the intensity contrast; and (2) we introduce a simple yet effective prior for adjusting the color saturation depending on the intensity contrast. The proposed method is tested with different kinds of images, compared with eight state-of-the-art methods: four enhancement methods and four haze removal methods. Experimental results show the proposed method can more effectively improve the visibility and preserve the naturalness of the images, as opposed to the compared methods. © 2016 Optical Society of America

**OCIS codes:** (100.2980) Image enhancement; (100.2000) Digital image processing; (010.1310) Atmospheric scattering; (100.2960) Image analysis; (100.0100) Image processing.

<https://doi.org/10.1364/JOSAA.34.000007>

## 1. INTRODUCTION

Image enhancement (IE) and image restoration (IR) play a critical role in outdoor vision applications, such as photography, surveillance systems, and intelligent vehicles using feature extraction [1–3]. Outdoor images usually suffer from different kinds of degradation factors, including inadequate illumination, nonuniform illumination, and scattering particles. Most existing methods are effective for some specific cases, but they often fail to improve the perceptual quality across a broad spectrum of situations. For instance, IE methods [4–15] are essentially employed to process the image of inadequate illumination, while IR methods [16–23] are mainly used to process the hazy image.

IE is a highly subjective process. IE methods are usually effective in improving the contrast, but they cannot handle the color saturation naturally. For example, histogram-based methods [4–9] and Retinex-based methods [11–13] enhance the image by stretching the contrast only, and the color saturation of the processed image looks lower than the original image.

To make the processed saturation look perceptually similar to the original saturation, some methods [24,25] compensate the saturation based on the pixel intensity, and some [26] adjust the saturation according to the global contrast, which unsteadily assume the saturation degradation is similar in different local areas. Also, others [27] enhance image contrast by combining global and local IE methods. In fact, the saturation degradation depends on particle scattering, which is closely related to the scene depth.

IR is mainly an objective process that involves various applications, such as noise and haze removal. Note that the focus of this paper is an attempt to develop a method that can be used for haze removal, not to justify or correct the noise. In general, it is hard to derive the haze from a single image, and therefore single image dehazing methods usually require strong priors or assumptions [16–23,28–30]. For example, He *et al.* [16] propose a simple dehazing method using the dark channel prior based on statistics. The prior is widely applied for color correction in various environments, such as in underwater images

[28]. Nishino *et al.* [19] treat the image as a factorial Markov random field, which assumes that the scene albedo and depth are two statistically independent latent layers. However, the priors and assumptions are usually effective in limited cases but not in common outdoor situations.

This task is rather challenging since it needs to consider more degradation factors than traditional methods. As the high-level semantics are various, it is impossible to propose a method that is effective for a broad variety of images by solving the problems deriving from high-level semantics. We know that hue, saturation, and intensity are three basic properties of color, which reflect the three basic characteristics for the human visual system (HVS) to perceive a color. Therefore, if we can manipulate the three properties well, our method should be applicable to a broad variety of images.

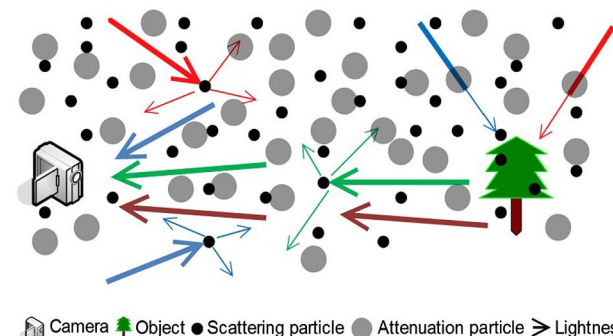
As the hue is usually in accordance with the real word [29], we mainly pay our attention to the processing of the intensity and the saturation. Our method enhances the intensity using the proposed content-adaptive histogram equalization and adjusts the color saturation according to the variation of the intensity contrast before and after intensity enhancement. The proposed method is tested on images with different degradation factors, including inadequate illumination, nonuniform illumination, or haze. Experimental results demonstrate that the proposed method can yield satisfactory results for a broad variety of images.

The main contributions of our work are as follows: (1) the content-adaptive histogram equalization (CAHE) is proposed to redistribute histogram components of the intensity; (2) a scheme of local contrast enhancement joint with the global intensity is designed to enhance details as well as prevent artifacts; (3) a simple but effective prior is utilized to adjust the color saturation based on the intensity contrast; and (4) from three criteria of color saturation naturalness, visibility level, and intensity naturalness, the proposed method is compared with four enhancement methods [conditional histogram equalization (CHE) [4], generalized unsharp masking (GUM) [10], naturalness preserved enhancement algorithm (NPEA) [11], and optimal contrast-tone mapping (OCTM) [14]] and four haze removal methods [the He *et al.* method [16], Tarel's method [17], the Bao *et al.* method [18], and the Nishino *et al.* method [19]].

The remainder of this paper is organized as follows. In Section 2, we explain the major causes of poor quality often seen in an outdoor image, and then we analyze the drawbacks of existing methods. Section 3 gives details of the proposed scheme of contrast enhancement. Section 4 presents the simple but efficient saturation adjustment based on intensity contrast. Section 5 shows the results of the proposed method compared with several methods commonly used in each field of image enhancement and restoration. In Section 6, we draw our conclusions.

## 2. OBSERVATION

In this section, we analyze the key factors that affect outdoor image quality and present our observations on existing problems. In general, the image quality is easily deteriorated by atmospheric particles and environment illuminations. As shown in Fig. 1, atmospheric particles can be classified into



Camera Object ● Scattering particle ● Attenuation particle ➤ Lightness

**Fig. 1.** Diagrammatic sketches of light transmission. The atmospheric particles mainly represent two models, being the attenuation model and the scattering model [31]. The attenuation model describes how the light is attenuated as it transmits from the scene point to the observer. The light scattering is due to the suspended scattering particles (e.g., dust and mist).

the attenuation model and the scattering model [31]. The attenuation model characterizes how the light is attenuated as it is transmitted in the scene. Light scattering is induced by suspended particles, such as dust and mist. In addition, the insufficient illumination under bad conditions (e.g., cloudy and nighttime scenes) is one of the serious factors that degrade outdoor image quality.

As light attenuation and illumination insufficiency (inadequate or nonuniform illumination) cause similar degradation, we take them as one kind of degradation factor. In general, there are mainly two kinds of degradation factors, i.e., illumination insufficiency and scattering particles, directly affecting the quality of an outdoor image. For example, the contrast of an outdoor image under rainy, cloudy, and nighttime scenes is low due to illumination insufficiency. The color saturation is visually unpleasant in the scene where the light is scattered by suspended particles.

Accordingly, existing methods can be grouped into two categories, i.e., image enhancement and image restoration. Enhancement methods are generally used to solve problems arising from illumination insufficiency, while restoration methods are mainly employed to process the image degraded by scattering particles. Conventional methods [4,10,11,14,16–19] are prone to suffer from the problems of overenhancement, underenhancement, or faint color, which directly affect the details and the color saturation of an image. Therefore, we analyze the limits and drawbacks of previous methods from two respects, i.e., detail presentation and saturation fidelity.

Details are essential to the visibility of an image. Many methods enhance the details of an image by improving the contrast. The classical histogram equalization (HE) method processes an image by equally distributing the histogram components [32], but it often maps two close gray levels to significantly different levels. To solve this problem of overenhancement, contrast-limited histogram equalization methods [5] are proposed to redistribute the histogram components using a fixed clip limit.

However, the existing contrast-limited methods do not take the characteristics of the HVS into consideration, so they cannot make the best use of the gray levels. For example, they

equally map the pixels to the gray level 0 and the gray level 127. In fact, the HVS perceives details differently depending on the illumination conditions. It is necessary to map more pixels to the gray levels that are more suitable for the HVS to perceive the details. Based on this observation, the proposed method sets the clip limit according to the characteristics of the HVS.

Color saturation is essential to the image naturalness. As mentioned in Section 1, IE methods cannot process the color saturation naturally, because the degradation of the color saturation is related to the particle scattering, but IE methods usually neglect the effect of the particle scattering. As for haze removal methods, the color saturation depends on the accuracy of the restoration model, which is usually a rough simulation. Therefore, the restored haze-free image usually suffers from oversaturation or faint color.

Similar to the observation by Tan [23] that an image taken in clear daylight conditions usually has more contrast than an image degraded by bad weather, we observe that a clear-day image has higher color saturation than an image degraded by bad-weather conditions. In general, as the scattering particles become heavier, both the color saturation and the local contrast decrease. Based on this observation, we assume that the saturation is monotonically related to the local contrast of the intensity. In other words, the saturation should be modified along with the contrast.

### 3. CONTRAST ENHANCEMENT

In this section, we present the details for contrast enhancement. First, we introduce the proposed CAHE, which is used to redistribute the histogram components of the intensity. Second, we give the scheme of local contrast enhancement joint with global intensity. By using the proposed method, we can enhance the contrast of the intensity naturally.

#### A. Content-Adaptive Histogram Equalization

The main idea of the CAHE is to stretch the gray levels as much as possible while preventing artifacts according to the just-noticeable-difference (JND) profile of the HVS. For the sake of hue preservation, the CAHE processes the intensity in the HSI color space. Let  $k$  indicate the input gray level. The mapping function  $f(k)$  of the classical HE is defined as

$$f(k) = \left( \sum_{i=0}^k b(i)/N \right) \cdot (M - 1), \quad (1)$$

where  $b(i)$  denotes the histogram component of the gray level  $i$ ,  $N$  denotes the total number of the pixels, and  $M$  is the number of gray levels. In the case that the gray-level distribution is highly localized, the mapping curve of Eq. (1) includes segments with high slopes. As a result, the classical HE usually maps two close gray levels to significantly different ones and results in overenhancement.

Contrast-limited adaptive histogram equalization (CLAHE) methods [5] can prevent overenhancement in a certain case by restricting the range of contrast using the clip limit. These methods use the same value for the clip limit  $\beta$  over all the gray levels. In fact, the HVS perceives the details of the image differently, depending on illumination conditions, and it is necessary to set the clip  $\beta$  limit according to the HVS perception.

In general, the HVS cannot perceive the luminance variation  $V(x, y)$  if the variation is less than the JND value [33–35]. The JND profile is related to the average background luminance  $B(x, y)$ , and its definition is given as

$$\text{JND}(x, y) = \begin{cases} T_0 \cdot \left( 1 - \sqrt{\frac{B(x, y)}{127}} \right) + 3 & \text{for } B(x, y) \leq 127, \\ \gamma \cdot (B(x, y) - 127) + 3 & \text{for } B(x, y) > 127, \end{cases} \quad (2)$$

where  $T_0$  is the visibility threshold when the gray levels of the background are zero, and  $\gamma$  denotes the slope of the line that models the function at higher background luminance. In this paper, the values of  $T_0$  and  $\gamma$  are set to 17 and 3/128, respectively, as mentioned in [33,34].

Experimental results show that CLAHE may cause unexpected artifacts for the gray levels having low JND values. On the contrary, if the clip limit is too low in the case that the JND value is high, the details cannot be enhanced sufficiently. For this reason, it is necessary to set the clip limit adaptively based on the HVS. In order to prevent artifacts while enhancing details as much as possible, the slope of the gray level  $k$  should be set equal to the corresponding JND value. Assuming the background luminance is similar to the pixel intensity, the clip limit  $\beta(k)$  of the gray level  $k$  can be derived as

$$\beta(k) = \text{JND}([f'(k)]), \quad (3)$$

where  $f'(k)$  is the mapping function of the clipped histogram components.

As the clip limit is unknown and  $f'(k)$  depends on the clipped histogram components, the process of redistributing the histogram components should alternate between calculating the clip limit and clipping the histogram components until none of the histogram components need further clipping. Therefore,  $f'(k)$  is given as follows:

$$f'(k) = \left( \sum_{i=0}^k b'(i)/N \right) \cdot (M - 1) \quad (4)$$

where  $k = 0, 1, \dots, L - 1$ ,

and  $b'(i)$  is the current histogram component of the gray level  $i$ . We summarize all the steps of the CAHE in Algorithm 1:

---

#### Algorithm 1: Content-Adaptive Histogram Equalization

---

- 1: Obtain the histogram of the intensity in the HSI color space.
  - 2: **repeat**
  - 3:   Map each gray level  $k$  using the function
$$f(k) = \left( \sum_{i=0}^k b(i)/N \right) \cdot (M - 1)$$
  - 4:   Obtain the extra counts of the histogram components beyond the limit
$$\beta(k) = \text{JND}([f'(k)])$$
  - 5:   Distribute the extra counts among the gray levels, whose new clip limits are less than their original counts, unless their counts are no less than their new clip limit.
  - 6:   Distribute the rest counts uniformly among the gray levels whose counts are less than their new clip limits.
  - 7: **until** none of the histogram components needs further clipping.
  - 8: Obtain the enhanced intensity using the clipped histogram.
-

## B. Local Enhancement Joint with Global Intensity

Since global image enhancement cannot enhance the details homogeneously in different areas, local enhancement is necessary in such cases. However, local enhancement methods usually result in overenhancement and confusion of the light source [11]. To overcome these problems, we devise a scheme of local enhancement joint with global intensity: (1) we modify the local histogram using the global histogram to prevent overenhancement; and (2) we preserve the relative lightness in different local areas according to their input intensity.

We first divide the image into nonoverlapping subareas of the empirical size of  $30 \times 30$ . Let  $D_1$  and  $D_2$  denote the width and height of the image, respectively. The number of the subareas is denoted as  $P \times Q$ , where  $P = [D_1/30]$  and  $Q = [D_2/30]$ . The entropy of the local histogram [36] is usually very low in the area where the local histogram is highly localized. In general, the lower the local entropy is, the more possible it is to result in overenhancement; therefore, the weight of the global histogram should be negatively related to the local entropy. We get the modified local histogram  $h_L^m$  as

$$h_L^m(i) = h_L(i)w + h_g(i)r(1 - w), \quad (5)$$

and

$$w = \min(1, e_L/e_g), \quad (6)$$

where  $h_L$  is the local histogram,  $h_g$  is the global histogram,  $e_L$  is the local entropy, and  $e_g$  is the global entropy.  $r$  denotes the ratio of the local pixel number to the global pixel number.

We obtain the mapping function  $f_l(x)$  for each local area  $l$  by using its modified local histogram  $h_L^m(i)$ . In order to preserve the relative lightness in different local areas, we take into consideration the input intensity in different areas. We obtain the local maximum image LM, whose pixels are the local maximum intensity of the corresponding local areas. We map LM using the bi-log transformation to get the mapped local maximum image LM' [11]. Then, we further modify the mapping function  $f_l(i)$  of the  $l$ th local area to get the modified mapping function  $g_l(x)$  as

$$g_l(k) = f_l(k) \cdot \text{LM}'_l \quad (7)$$

where  $\text{LM}'_l$  is the mapped local maximum intensity of the  $l$ th local area.

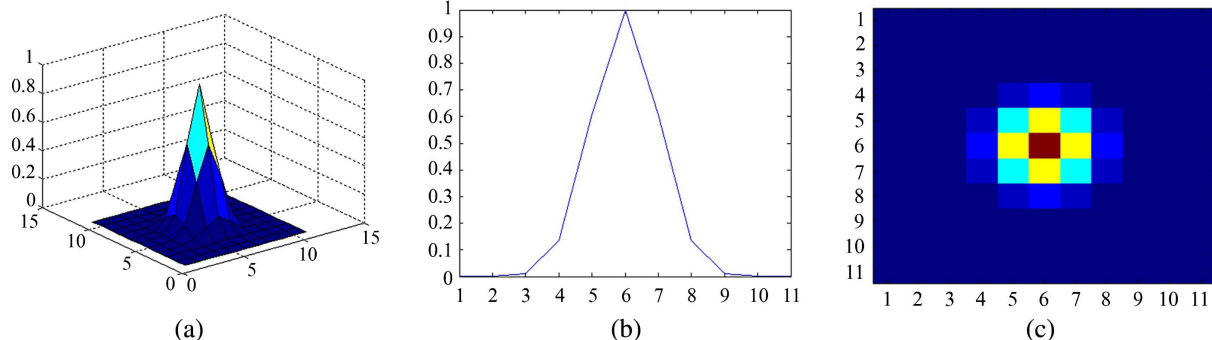


**Fig. 2.** Illustration of the near-local areas. (a) The surf of the weights. (b) The 2D illustration of the weights. (c) The nine areas nearest to the pixel are applied to refine the mapping result. The nine nearest areas include the center area, four connected areas, and four areas in the diagonal directions.

Since the independent processing of nonoverlapping subareas often produces an undesirable checkerboard effect, we subsequently eliminate the checkerboard effect using a Gaussian filter. We assume that the mapping function of the  $l$ th area transforms the gray level  $k$  to the gray level  $k_l^m$ . For a pixel of gray level  $k$  at  $(x, y)$ , we obtain its refined mapping result  $L_e(x, y)$  as follows:

$$L_e(x, y) = \frac{1}{W} \cdot \sum_{l=1}^{SN} \left( \exp\left(-\frac{(x - x_l)^2 + (y - y_l)^2}{2\sigma^2}\right) \cdot k_l^m \right), \quad (8)$$

where  $k_l^m$  represents the modified gray level,  $\sigma$  is empirically set as 30,  $(x_l, y_l)$  is the center of the  $l$ th area, SN is the number of the near areas taken into calculation, and  $W$  is the normalization factor given by

$$W = \sum_{l=1}^{SN} \exp\left(-\frac{(x - x_l)^2 + (y - y_l)^2}{2\sigma^2}\right). \quad (9)$$

In the case that the image size is very large, the input image is divided into many subareas. The computation of Eq. (8) is intensive if we take all the subareas into consideration. However, the weight decreases quickly as the distance increases as Fig. 2(c) shows. It is easy to verify that the nine nearest local areas take up about 80% of the total weight. Therefore, we only take into consideration the nine nearest local areas to speed up the computation.

Figure 3 illustrates the comparison of the intensity enhancement between our method and CLAHE [5]. As shown in Fig. 3, both the proposed method and CLAHE can enhance the details obviously. However, CLAHE results in artifacts in the sky area due to overenhancement. As the proposed method adaptively sets the clipping limit based on the HVS, our result seems to be more natural.

## 4. CONTRAST-DEPENDENT COLOR SATURATION ADJUSTMENT

As mentioned in Section 2, the color saturation is monotonically related to the contrast. Therefore, the color saturation should be adjusted after applying contrast enhancement; otherwise, it may produce an unnatural-looking image. In this

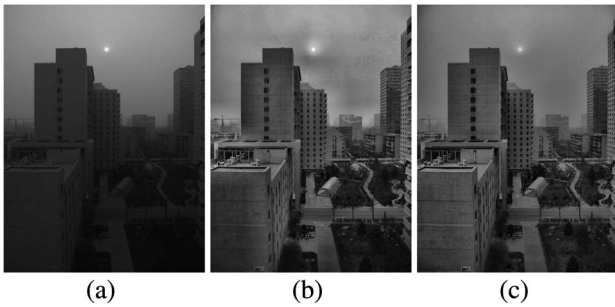


**Fig. 3.** Comparison of contrast enhancement. (a) The input image. (b) The result of CLAHE [5]. (c) Our result. The result of CLAHE has artifacts in the sky area, while our method enhances the image without artifacts.

section, we introduce a new method of contrast-dependent color saturation adjustment (CDCSA) as shown in Fig. 4.

#### A. Calculation of the Contrast Ratio

CDCSA measures the contrast variation using the ratio between local contrast of the processed intensity and the input intensity. It is obvious that the local contrast ratio is related to the size of the local area. Our explorations lead us to the notion that the maximum ratio is optimal for color saturation adjustment. However, the computational cost to get the maximum ratio is intensive because the local area size is various. Experimental results show the optimal result is similar to the result when the area size is set as  $11 \times 11$ . Therefore, we set the local area size as  $11 \times 11$  to calculate the contrast.

Let  $L_{\max}$  and  $L_{\min}$  respectively denote the maximum intensity and the minimum intensity of the local area centered at  $(x, y)$ , and we can get the local contrast  $C(x, y)$  according to the Michelson formula [37,38]

$$C(x, y) = \frac{L_{\max}(x, y) - L_{\min}(x, y)}{L_{\max}(x, y) + L_{\min}(x, y)}. \quad (10)$$

Similarly, we get the local contrast  $C_e(x, y)$  of the enhanced intensity. Then, we get the ratio of  $C_e(x, y)$  and  $C(x, y)$  as follows:

$$R = \frac{C_e(x, y)}{C(x, y)}. \quad (11)$$

The contrast is very small in the smooth area, where the local minimum is close to the local maximum. In such cases, the denominator of Eq. (11) is close to zero, and the contrast ratio

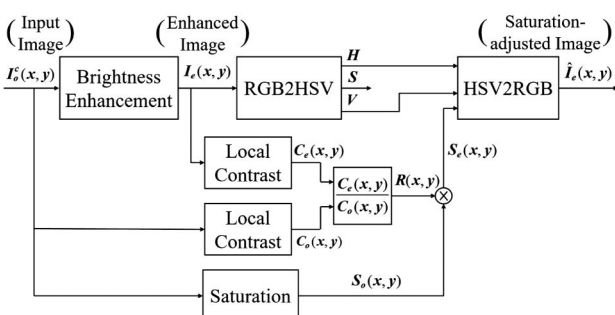


**Fig. 4.** Block diagram of the proposed color saturation adjustment algorithm.

$R$  is prone to suffer from noises. To avoid  $C(x, y)$  being too small, we empirically set the lower bound of  $C(x, y)$  as  $C_l = 0.2$ . When the denominator of Eq. (11) is lower than or equal to  $C_l$ , we add  $\Delta(x, y) = C_l - C(x, y)$  to the denominator and the numerator. Then, we derive the following equation:

$$R(x, y) = \begin{cases} \frac{C_e(x, y)}{C(x, y)} & \text{for } C(x, y) > C_l, \\ \frac{C_e(x, y) + \Delta(x, y)}{C(x, y) + \Delta(x, y)} & \text{for } C(x, y) \leq C_l. \end{cases} \quad (12)$$

#### B. Color Saturation Adjustment

As mentioned previously, our method mainly solves the problems arising from attenuation and atmospheric scattering. The light attenuation is multiplicative degradation, and the atmospheric is additive degradation. The enhanced image  $I_e^c(x, y)$  is a transformation of the input image  $I_o^c(x, y)$  adjusted by a multiplicative factor and an additive factor as follows:

$$I_e^c(x, y) = A \cdot I_o^c(x, y) + B, \quad (13)$$

where  $A$  denotes the multiplicative factor,  $B$  denotes the additive factor, and  $c \in (r, g, b)$  denotes the color channel.

According to the definition of saturation in the HSI color space, the original saturation is given by

$$S_o(x, y) = 1 - \frac{3 \cdot \min_{c \in (r, g, b)} I_o^c(x, y)}{\sum_{c \in (r, g, b)} I_o^c(x, y)}. \quad (14)$$

The saturation of the enhanced image is given by

$$S_e(x, y) = 1 - \frac{3 \cdot \min_{c \in (r, g, b)} I_e^c(x, y)}{\sum_{c \in (r, g, b)} I_e^c(x, y)}. \quad (15)$$

Accordingly, we can get the ratio  $R_s(x, y)$  between the enhanced saturation  $S_e(x, y)$  and the original saturation  $S_o(x, y)$ :

$$R_s(x, y) = \frac{A \cdot I_{\text{mean}}(x, y)}{A \cdot I_{\text{mean}}(x, y) + B}, \quad (16)$$

where

$$I_{\text{mean}}(x, y) = \sum_{c \in (r, g, b)} I_o^c(x, y) / 3. \quad (17)$$

In a local area, pixels are affected by the similar multiplicative factor  $A$  and the additive factor  $B$ . We can rewrite the contrast ratio of Eq. (12) as

$$R_s(x, y) = \frac{A \cdot I_{\max}(x, y)}{A \cdot I_{\max}(x, y) + B}, \quad (18)$$

where

$$I_{\max}(x, y) = \max_{c \in (r, g, b)} \left( \max_{(i, j) \in \Omega(x, y)} I_o^c(x, y) / 3 \right). \quad (19)$$

From Eqs. (16) and (18), we can see that the saturation is monotonically and positively related to the local contrast. For simplicity, we can adjust the saturation  $S_e(x, y)$  as follows:

$$S_e(x, y) = (a \cdot \{R(x, y)\}^\alpha + b) \cdot S_o(x, y), \quad (20)$$

where  $S_e(x, y)$  is the adjusted saturation,  $a$  and  $b$  are two key parameters respectively for scaling and shifting, and  $\alpha$  is used to make the equation more general.

According to our observation mentioned in Section 2, we can derive that (1) the saturation should be preserved in the case where the contrast has no change, and (2) the saturation

should be set to zero in the case where the contrast of nonzero values becomes zero. Accordingly, we derive (1)  $a + b = 1$ , and (2)  $b = 0$ . However, it is hard to derive the parameter  $\alpha$  theoretically. We experimentally find that the method performs the best when  $\alpha$  is close to 1, and therefore we set  $\alpha$  to 1 throughout the remainder of this paper. As a result, Eq. (20) can be simplified as

$$S_e(x, y) = R(x, y) \cdot S_o(x, y). \quad (21)$$

## 5. EXPERIMENTS AND DISCUSSION

We have tested the proposed method on various images of inadequate illumination, nonuniform illumination, or haze.

To assess the effectiveness, we compare the proposed method with eight state-of-the-art methods, including four enhancement methods: CHE [4], GUM [10], NPEA [11], and OCTM [14]; as well as four haze removal methods: the He *et al.* method [16], Tarel's method [17], the Bao *et al.* method [18], the Nishino *et al.* method [19], the Meng *et al.* method [39], and the Berman *et al.* method [40]. These methods are selected according to the number of citations and the latest techniques.

The major parameters of the compared algorithms are set as follows: for GUM, the adaptive gain is utilized with the maximum gain set as 5 and the contrast enhancement factor is 0.005; for OCTM, the image is divided into  $6 \times 6$  local areas, no six consecutive bins are all empty, and each bin has at most

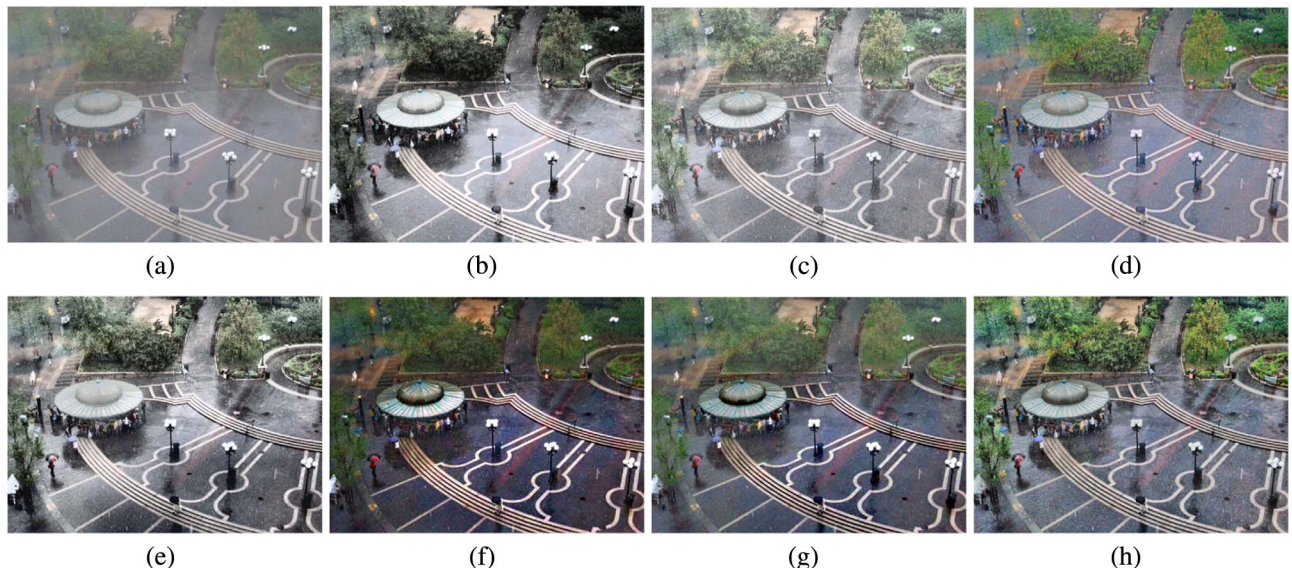


**Fig. 5.** Results for image *Rain*. (a) Input image. (b) The result of CHE [4]. (c) The result of GUM [10]. (d) The result of NPEA [11]. (e) The result of OCTM [14]. (f) The result of the Meng *et al.* method [39]. (g) The result of the Berman *et al.* method [40]. (h) Our result. This rainy image is taken from [41].

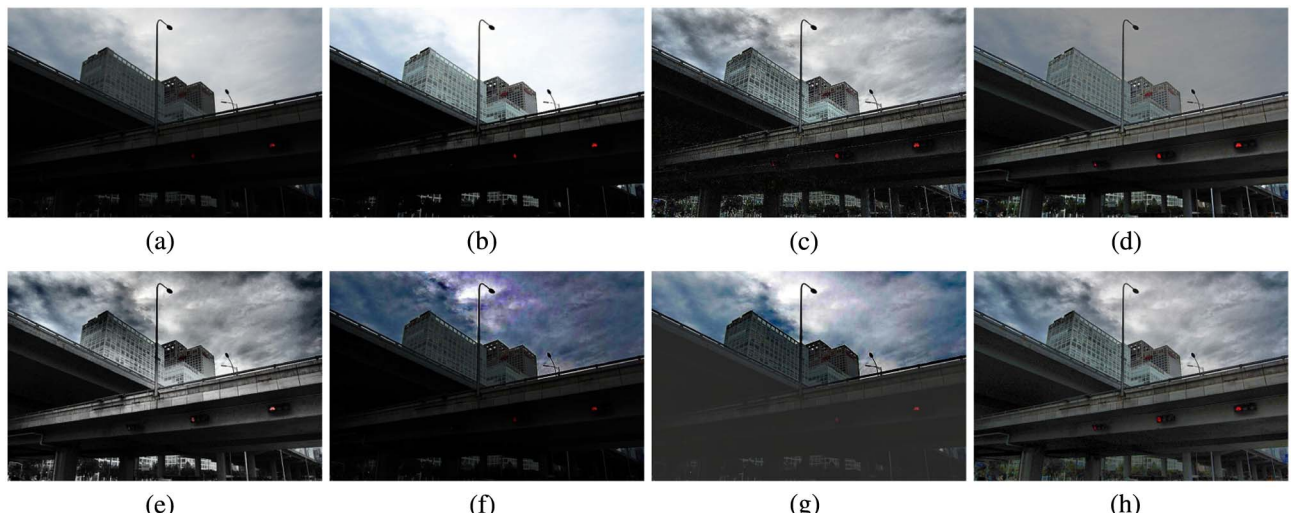


**Fig. 6.** Results for image *Bridge* in our dataset. (a) Input image. (b) The result of CHE [4]. (c) The result of GUM [10]. (d) The result of NPEA [11]. (e) The result of OCTM [14]. (f) The result of the Meng *et al.* method [39]. (g) The result of the Berman *et al.* method [40]. (h) Our result.

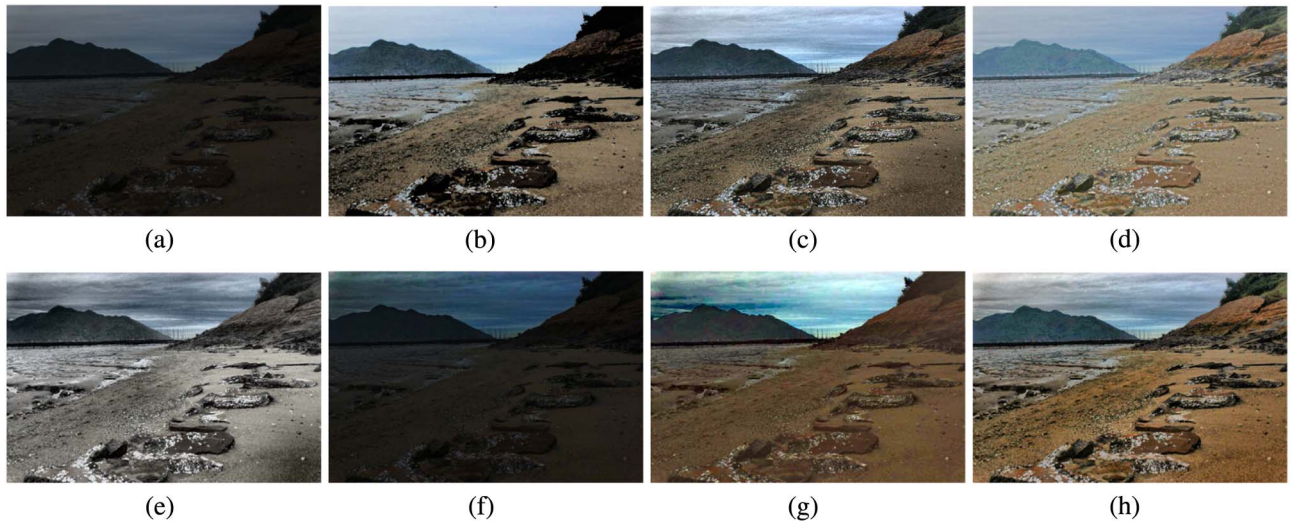


**Fig. 7.** Results for image *Beach*. (a) Input image. (b) The result of CHE [4]. (c) The result of GUM [10]. (d) The result of NPEA [11]. (e) The result of OCTM [14]. (f) The result of the Meng *et al.* method [39]. (g) The result of the Berman *et al.* method [40]. (h) Our result. This test image is taken from [42].

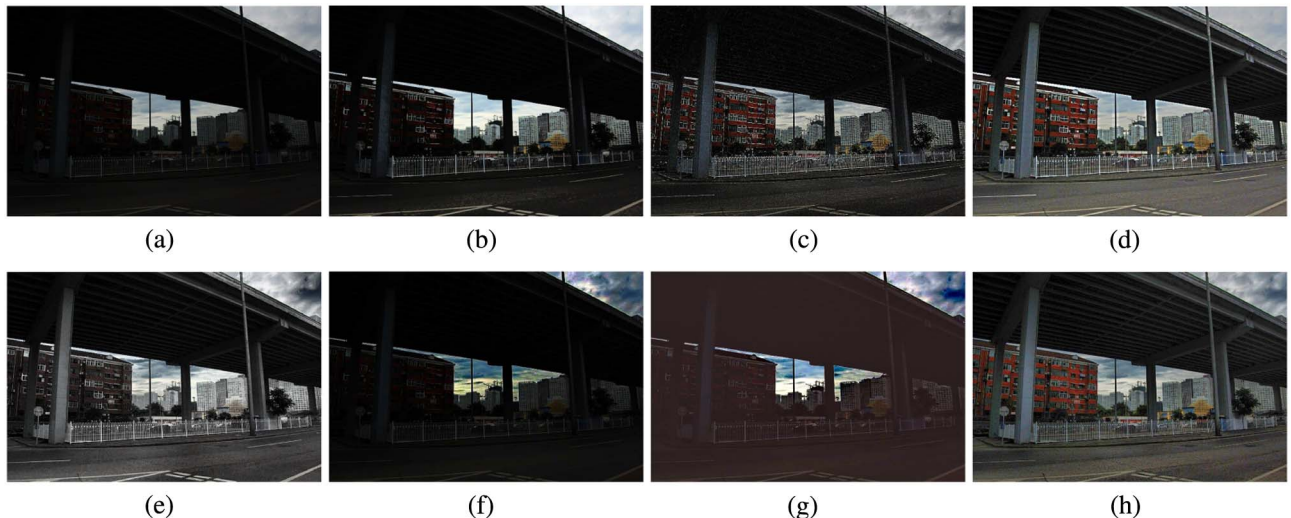


**Fig. 8.** Results for image *Highway* in our dataset. (a) Input image. (b) The result of CHE [4]. (c) The result of GUM [10]. (d) The result of NPEA [11]. (e) The result of OCTM [14]. (f) The result of the Meng *et al.* method [39]. (g) The result of the Berman *et al.* method [40]. (h) Our result.

six steps; the parameters of the other methods are set as the paper provided. For an in-depth description of the parameters, we refer the reader to the literature [4,10,11,14,16–19].

Due to the space limitation, we present eight representatives, including four cloudy images and four hazy images. We assess the results from three criteria: (1) the color saturation naturalness, (2) the visibility level, and (3) the intensity naturalness. Since there is no objective metric to assess the color saturation naturalness, we subjectively evaluate the color saturation naturalness. For the visibility level and the intensity naturalness, we adapt the visibility-level descriptor (VLD) [43] and the lightness-order error (LOE) metric [11], respectively. VLD demonstrates the contrast improvement [43]. A higher VLD value indicates that the image has more details. LOE

**Table 1. Quantitative Measurement Results of the Visibility Level Descriptor**

| Method | Image |        |       |         |         |
|--------|-------|--------|-------|---------|---------|
|        | Rain  | Bridge | Beach | Highway | Average |
| Orig.  | 1     | 1      | 1     | 1       | 1       |
| CHE    | 2.95  | 1.21   | 4.12  | 2.06    | 2.58    |
| GUM    | 3.43  | 5.94   | 6.54  | 6.28    | 5.55    |
| NPEA   | 2.13  | 4.23   | 4.38  | 6.19    | 4.23    |
| OCTM   | 4.00  | 4.05   | 5.66  | 5.23    | 4.73    |
| Our    | 3.87  | 4.95   | 5.66  | 6.21    | 5.17    |

**Table 2. Quantitative Measurement Results of the Lightness-Order Error**

| Method | Image |        |       |         |         |
|--------|-------|--------|-------|---------|---------|
|        | Rain  | Bridge | Beach | Highway | Average |
| Orig.  | 0     | 0      | 0     | 0       | 0       |
| CHE    | 3.72  | 1.00   | 3.18  | 0.67    | 2.14    |
| GUM    | 18.89 | 22.68  | 18.35 | 15.75   | 18.92   |
| NPEA   | 9.93  | 14.47  | 33.13 | 13.87   | 17.85   |
| OCTM   | 19.08 | 15.77  | 29.55 | 6.8710  | 17.8177 |
| Our    | 12.56 | 6.81   | 10.25 | 7.17    | 9.20    |

recently proposed in [11] measures the intensity naturalness by the relative order of lightness in different local areas. A lower LOE value represents that the lightness order is better preserved.

#### A. Test on the Images of Inadequate or Nonuniform Illumination

We first test the proposed method compared with CHE, GUM, NPEA, and OCTM over the test images of inadequate and nonuniform illumination, as illustrated in Figs. 5–8. We can see that the color saturation of the results processed by CHE, GUM, and OCTM seems to be faded. As the example

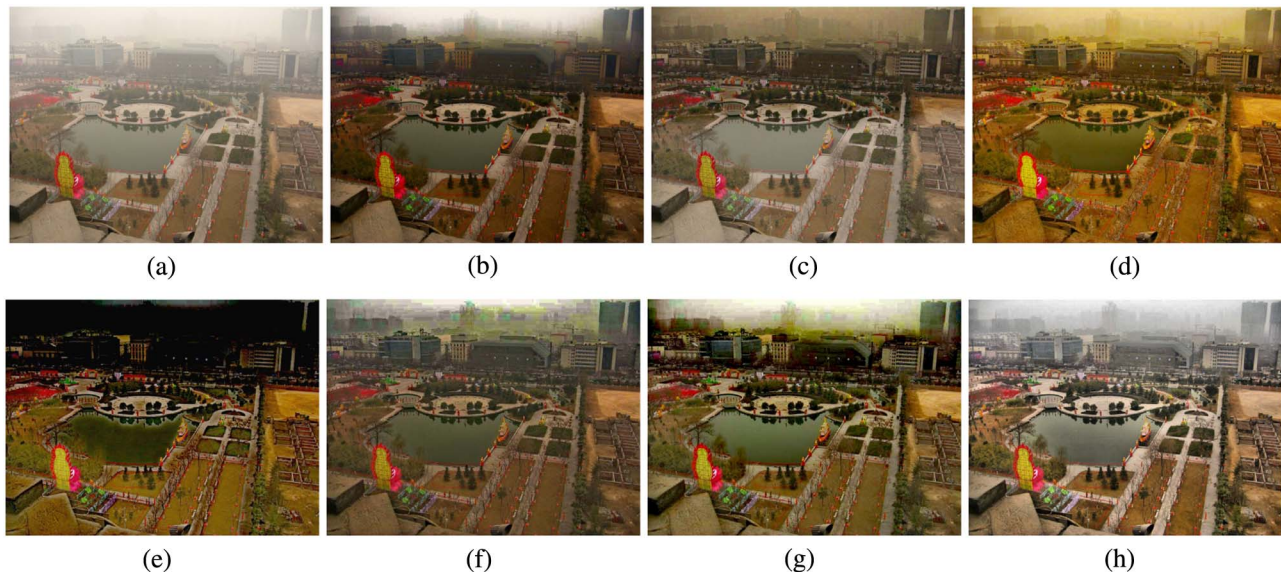


**Fig. 9.** Results for image *Park* in our dataset. (a) Input image. (b) The result of He's method [16]. (c) The result of Tarel's method [17]. (d) The result of Bao's method [18]. (e) The result of the Nishino *et al.* method [19]. (f) The result of the Meng *et al.* method [39]. (g) The result of the Berman *et al.* method [40]. (h) Our result.

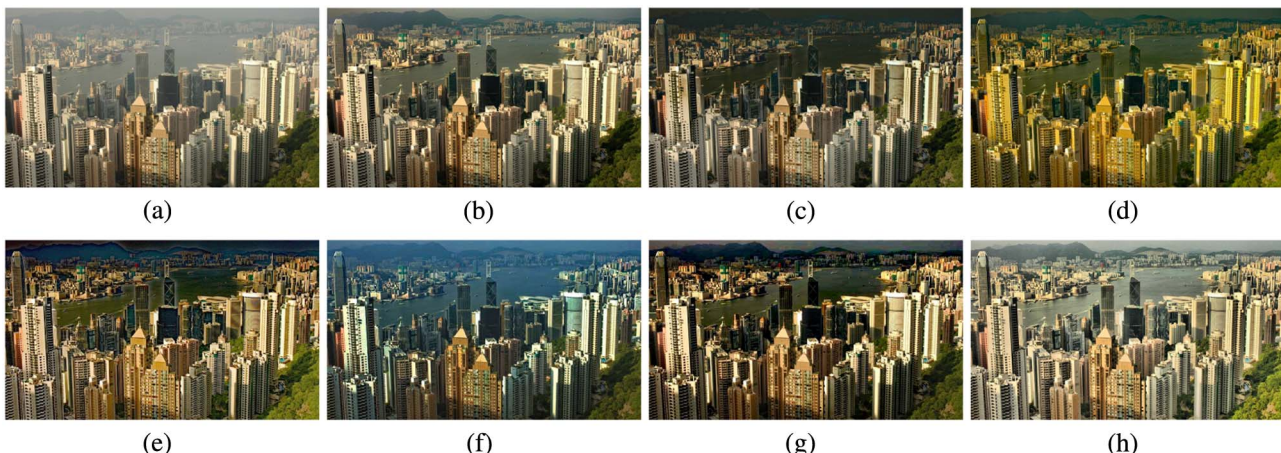


**Fig. 10.** Results for image *Hong Kong* taken from [16]. (a) Input image. (b) The result of He's method [16]. (c) The result of Tarel's method [17]. (d) The result of Bao's method [18]. (e) The result of the Nishino *et al.* method [19]. (f) The result of the Meng *et al.* method [39]. (g) The result of the Berman *et al.* method [40]. (h) Our result.

shows in Fig. 8(d), NPEA produces slightly better color saturation. However, especially for the distant regions in Fig. 7(d), NPEA yields an unnatural-looking image. As can be seen in Figs. 5–8, the proposed method for the color saturation should be able to yield not just comparable but even better results.

Tables 1 and 2, respectively, show VLD and LOE of all the tested images. From Table 1, we can see that GUM is the best, our method being second at contrast enhancement. However, GUM cannot preserve the intensity naturalness well. On the contrary, as a global method, CHE is the best at preserving the lightness order. CHE performs the worst at contrast enhancement. As shown in Tables 1 and 2, our method not only

preserves the lightness order but also enhances the contrast significantly.

## B. Test on Hazy Images

To further illustrate the effectiveness of the proposed method, the proposed method is compared with four state-of-the-art haze removal methods: the He *et al.* method [16], Tarel's method [17], the Bao *et al.* method [18], the Nishino *et al.* method [19], the Meng *et al.* method [39], and the Berman *et al.* method [40]. Results of these methods are shown in Figs. 9–12. It can be seen in Figs. 9(b) and 12(b) that the results of the He *et al.* method are oversaturated across the entire

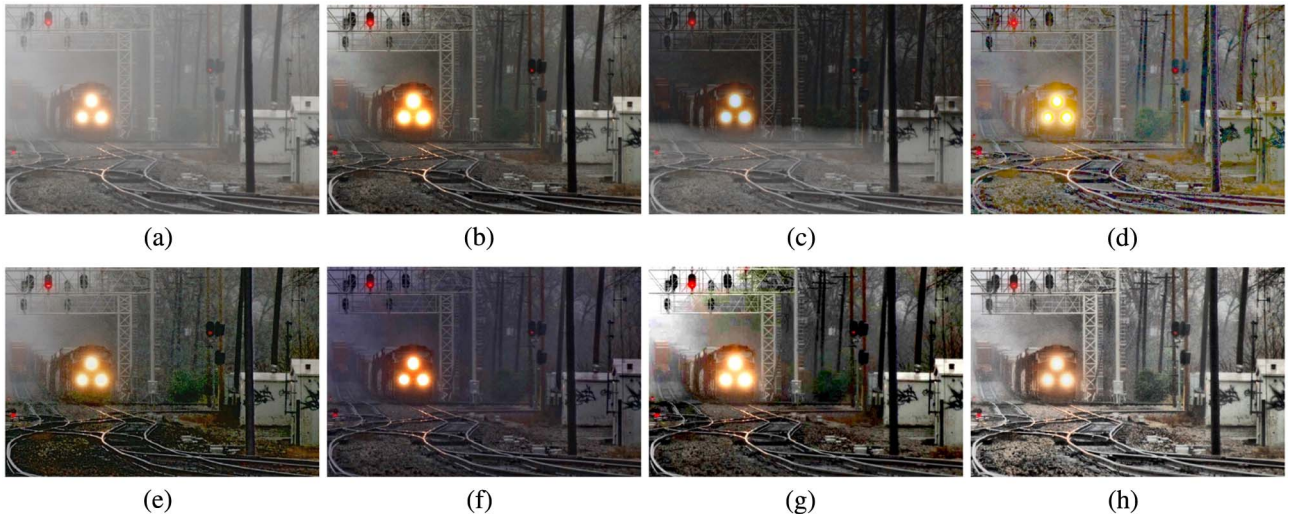


**Fig. 11.** Results for image *Train* taken from [16]. (a) Input image. (b) The result of He's method [16]. (c) The result of Tarel's method [17]. (d) The result of Bao's method [18]. (e) The result of the Nishino *et al.* method [19]. (f) The result of the Meng *et al.* method [39]. (g) The result of the Berman *et al.* method [40]. (h) Our result.

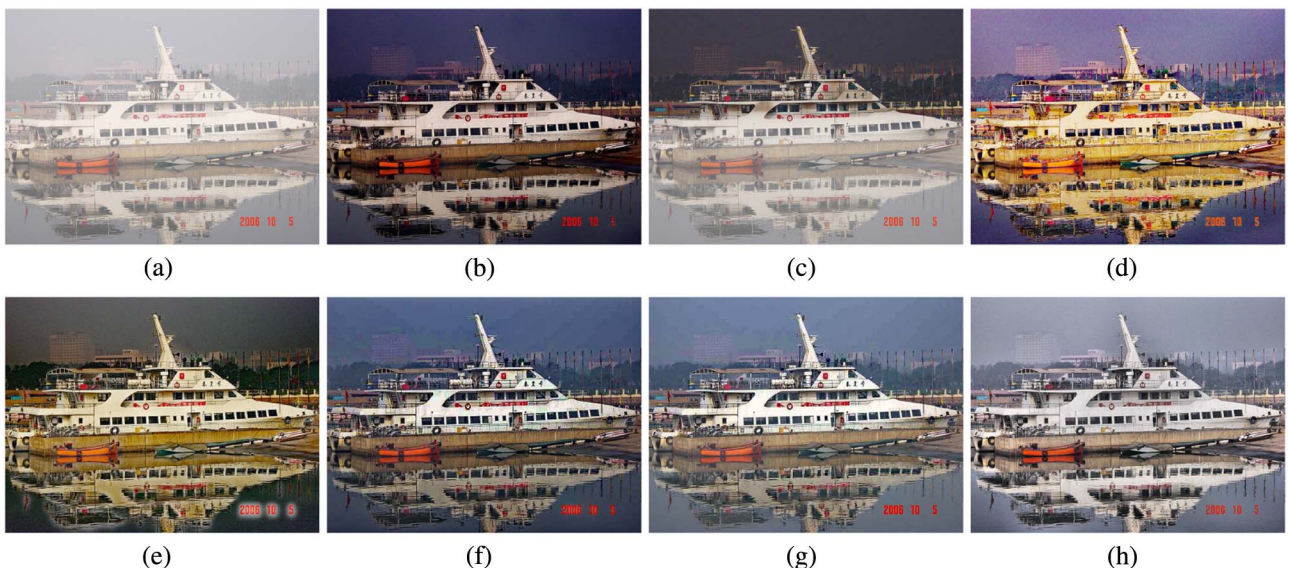


**Fig. 12.** Results for image *Ship* in our dataset. (a) Input image. (b) The result of He's method [16]. (c) The result of Tarel's method [17]. (d) The result of Bao's method [18]. (e) The result of the Nishino *et al.* method [19]. (f) The result of the Meng *et al.* method [39]. (g) The result of the Berman *et al.* method [40]. (h) Our result.

**Table 3. Quantitative Measurement Results of the Visibility Level Descriptor**

| Method  | Image |           |       |      |         |
|---------|-------|-----------|-------|------|---------|
|         | Park  | Hong Kong | Train | Ship | Average |
| Orig.   | 1     | 1         | 1     | 1    | 1       |
| He      | 1.21  | 1.47      | 1.92  | 2.08 | 1.67    |
| Tarel   | 1.58  | 1.50      | 1.72  | 1.81 | 1.65    |
| Bao     | 1.89  | 1.47      | 3.04  | 4.25 | 2.66    |
| Nishino | 2.43  | 2.65      | 3.18  | 3.66 | 2.98    |
| Our     | 2.43  | 2.29      | 4.28  | 2.82 | 2.95    |

**Table 4. Quantitative Measurement Results of the Lightness-Order Error**

| Method  | Image |           |       |       |         |
|---------|-------|-----------|-------|-------|---------|
|         | Park  | Hong Kong | Train | Ship  | Average |
| Orig.   | 0     | 0         | 0     | 0     | 0       |
| He      | 18.62 | 2.69      | 11.97 | 9.51  | 10.70   |
| Tarel   | 43.38 | 11.05     | 36.71 | 14.95 | 26.52   |
| Bao     | 20.65 | 12.51     | 26.75 | 8.39  | 17.08   |
| Nishino | 48.09 | 10.29     | 11.99 | 10.67 | 20.26   |
| Our     | 20.03 | 8.07      | 14.90 | 10.90 | 13.47   |

images. Color saturation by Tarel's method overly varies in different local areas, as illustrated in Figs. 9–12(c). As can be seen in Figs. 9–12(d), Bao *et al.* results also seem to be unnatural due to the oversaturation in some objects. Comparatively, it can be observed that the proposed method is able to yield more natural images for examples in Figs. 9–12(h).

In order to objectively evaluate the visibility level and the intensity naturalness, we also evaluate VLD and LOE. We make all the pairwise comparisons among the algorithms on each different haze image and show the results in Tables 3 and 4. From Table 3, it can be seen that Nishino *et al.* is the best, while our method is the second best at contrast enhancement. However, the results of the Nishino *et al.* method show overenhancement in some areas, as depicted in Figs. 9(e) and 10(e). The LOE value of the He *et al.* method is similar if not better than that of our method, though the He *et al.* method performs the worst when tested to enhance the contrast. As a result, our method not only preserves the lightness order effectively but also enhances the contrast.

## 6. CONCLUSIONS

In this paper, we proposed an image enhancement method, which is applicable to enhance outdoor images, including a non-uniform illumination image, an inadequate illumination image, and a hazy image. The experimental results of the proposed method demonstrate that it is practicable to enhance a broad variety of images by improving the intensity contrast and by adjusting the color saturation. The effectiveness of the proposed method has been evaluated from three criteria: (1) the color saturation naturalness, (2) the visibility level, and (3) the intensity naturalness. For more information about the test images and our open software, please contact the authors for support.

The model of our method to adjust the color saturation is derived from multiple experiments. We believe that there should be a theoretical formula to adjust the color saturation in accordance with our model. We leave this work for our future research.

**Funding.** Ministry of Science, ICT and Future Planning (MSIP) (B0101-16-0525); Ministry of Trade, Industry and Energy (MOTIE) (10047788).

**Acknowledgment.** We would like to thank Jacob D'Avy for his helpful feedback. Special thanks go to the anonymous reviewers of this paper for their constructive comments.

## REFERENCES

1. H. Lee, S. Jeon, I. Yoon, and J. Paik, "Recent advances in feature detectors and descriptors," *IEIE Trans. Smart Process. Comput.* **5**, 153–163 (2016).
2. Y. Kim, S. Jeong, J. Oh, and S. Lee, "Fast MOG (mixture of Gaussian) algorithm based on predicting model parameters," *J. Arts Imaging Sci.* **2**, 41–45 (2015).
3. J. Im and J. Paik, "Spatially adaptive histogram equalization for single image-based ghost-free high dynamic range imaging," *J. Arts Imaging Sci.* **1**, 55–59 (2014).
4. T. Arici, S. Dikbas, and Y. Altunbasak, "A histogram modification framework and its application for image contrast enhancement," *IEEE Trans. Image Process.* **18**, 1921–1935 (2009).
5. A. M. Reza, "Realization of the contrast limited adaptive histogram equalization (CLAHE) for real-time image enhancement," *J. VLSI Signal Process. Syst. Signal Image Video Technol.* **38**, 35–44 (2004).
6. H. Zhu, F. H. Chan, and F. K. Lam, "Image contrast enhancement by constrained local histogram equalization," *Comput. Vis. Image Understanding* **73**, 281–290 (1999).
7. K. Zuiderveld, "Contrast limited adaptive histogram equalization," in *Graphics Gems*, IVth ed. (Academic, 1994), pp. 474–485.
8. Z. Chen, B. R. Abidi, D. L. Page, and M. A. Abidi, "Gray-level grouping (GLG): an automatic method for optimized image contrast enhancement—Part I: the basic method," *IEEE Trans. Image Process.* **15**, 2290–2302 (2006).
9. K. Huang, Q. Wang, and Z. Wu, "Natural color image enhancement and evaluation algorithm based on human visual system," *Comput. Vis. Image Understanding* **103**, 52–63 (2006).
10. G. Deng, "A generalized unsharp masking algorithm," *IEEE Trans. Image Process.* **20**, 1249–1261 (2011).
11. S. Wang, J. Zheng, H. Hu, and B. Li, "Naturalness preserved enhancement algorithm for non-uniform illumination images," *IEEE Trans. Image Process.* **22**, 3538–3548 (2013).
12. E. Provenzi, C. Gatta, M. Fierro, and A. Rizzi, "A spatially variant white-patch and gray-world method for color image enhancement driven by local contrast," *IEEE Trans. Pattern Anal. Mach. Intell.* **30**, 1757–1770 (2008).
13. J. M. Morel, A. B. Petro, and C. Sbert, "A PDE formalization of retinex theory," *IEEE Trans. Image Process.* **19**, 2825–2837 (2010).
14. X. Wu, "A linear programming approach for optimal contrast-tone mapping," *IEEE Trans. Image Process.* **20**, 1262–1272 (2010).
15. S. Lee, D. Zhang, and S. Ko, "Image contrast enhancement based on a multi-cue histogram," *IEIE Trans. Smart Process. Comput.* **4**, 349–353 (2015).
16. K. He, J. Sun, and X. Tang, "Single image haze removal using dark channel prior," *IEEE Trans. Pattern Anal. Mach. Intell.* **33**, 2341–2353 (2010).
17. J. Tarel, N. Hautiere, A. Cord, D. Gruyer, and H. Halmaoui, "Improved visibility of road scene images under heterogeneous fog," in *IEEE Intelligent Vehicles Symposium (IV)* (IEEE, 2010), pp. 478–485.
18. L. Bao, Y. Song, Q. Yang, and N. Ahuja, "An edge-preserving filtering framework for visibility restoration," in *International Conference on Pattern Recognition (ICPR)* (IEEE, 2012), pp. 384–387.

19. K. Nishino, L. Kratz, and S. Lombardi, "Bayesian defogging," *Int. J. Comput. Vision* **98**, 263–278 (2012).
20. J.-P. Tarel and N. Hautière, "Fast visibility restoration from a single colour or gray level image," in *IEEE International Conference on Computer Vision* (IEEE, 2009), pp. 2201–2208.
21. R. Fattel, "Single image dehazing," *ACM Trans. Graphics (TOG)* **27**, 1–9 (2008).
22. C. O. Ancuti and C. Ancuti, "Single image dehazing by multi-scale fusion," *IEEE Trans. Image Process.* **22**, 3271–3282 (2013).
23. R. T. Tan, "Visibility in bad weather from a single image," in *IEEE Conference on Computer Vision and Pattern Recognition* (IEEE, 2008), pp. 1–8.
24. H. Fuchsberger, "Method of correcting color saturation in electronic image processing," U.S. patent 4831434 A (May 16, 1989).
25. A. C. Gallagher and E. E. Gindele, "Method for compensating image color when adjusting the contrast of a digital color image," U.S. patent 6438264 B1 (August 20, 2002).
26. O. Pirinen, A. Foi, and A. Gotchev, "Color high dynamic range (HDR) imaging in luminance-chrominance space," in *International Workshop on Video Processing and Quality Metrics for Consumer Electronics* (Ira A. Fulton Schools of Engineering, 2007), pp. 121–124.
27. K. Song, H. Kang, and M. Kang, "Hue-preserving and saturation-improved color histogram equalization algorithm," *J. Opt. Soc. Am. A* **33**, 1076–1088 (2016).
28. H. Lu, Y. Li, L. Zhang, and S. Serikawa, "Contrast enhancement for images in turbid water," *J. Opt. Soc. Am. A* **32**, 886–893 (2015).
29. B. Li, S. Wang, J. Zheng, and L. Zheng, "Single image haze removal using content-adaptive dark channel and post enhancement," *IET Comput. Vis.* **8**, 131–140 (2014).
30. R. C. Henry, S. Mahadev, S. Urquijo, and D. Chitwood, "Color perception through atmospheric haze," *J. Opt. Soc. Am. A* **17**, 831–835 (2000).
31. S. G. Narasimhan and S. K. Nayar, "Contrast restoration of weather degraded images," *IEEE Trans. Pattern Anal. Mach. Intell.* **25**, 713–724 (2003).
32. S. G. Narasimhan and S. K. Nayar, "Vision and the atmosphere," *Int. J. Comput. Vis.* **48**, 233–254 (2002).
33. R. C. Gonzalez, R. E. Woods, and S. L. Eddins, *Digital Image Processing* (Prentice Hall, 2004).
34. C.-H. Chou and Y.-C. Li, "A perceptually tuned subband image coder based on the measure of just-noticeable-distortion profile," *IEEE Trans. Circuits Syst. Video Technol.* **5**, 467–476 (1995).
35. S. Jung, "Exact histogram specification considering the just noticeable difference," *IEIE Trans. Smart Process. Comput.* **3**, 52–58 (2014).
36. J. N. Kapur, P. K. Sahoo, and A. K. C. Wong, "A new method for gray-level picture thresholding using the entropy of the histogram," *Comput. Vision Graph. Image Process.* **29**, 273–285 (1985).
37. M. I. Sezan, K.-I. Yip, and S. J. Daly, "Uniform perceptual quantization: applications to digital radiography," *IEEE Trans. Syst. Man Cybern.* **17**, 622–634 (1987).
38. E. Peli, "Contrast in complex images," *J. Opt. Soc. Am. A* **7**, 2032–2040 (1990).
39. G. Meng, Y. Wang, J. Duan, S. Xiang, and C. Pan, "Efficient image dehazing with boundary constraint and contextual regularization," in *IEEE Conference on Computer Vision and Pattern Recognition* (IEEE, 2013), pp. 617–624.
40. D. Berman, T. Treibitz, and S. Avidan, "Non-local image dehazing," in *IEEE Conference on Computer Vision and Pattern Recognition* (IEEE, 2016), pp. 1–9.
41. <https://nummynims.wordpress.com/tag/rainy-day>.
42. <http://www.mafengwo.cn/i/1075506.html>.
43. N. Hautière, J.-P. Tarel, D. Aubert, and E. Dumont, "Blind contrast enhancement assessment by gradient rationing at visible edges," *Image Anal. Stereol.* **27**, 87–95 (2008).